

# Seismic images of crust and upper mantle in Central Iran (from Jiroft to Ashtian) via teleseismic waves

Shahireh JAVADI<sup>1</sup>, Fataneh TAGHIZADEH-FARAHMAND<sup>2,\*</sup> ,  
Mohammad Reza GHEITANCHI<sup>3</sup>

<sup>1</sup> Department of Geophysics, North Tehran Branch, Islamic Azad University, Tehran, Iran

<sup>2</sup> Department of Physics, Qom Branch, Islamic Azad University, Qom, Iran

<sup>3</sup> Department of Geophysics, Tehran University, Tehran, Iran

**Abstract:** A detailed knowledge of the thickness of crust and upper mantle structure is important for understanding a plate tectonics and geodynamics in the region. We use body wave for detecting details of the subsurface structure. The information in this research is collected from a seismic linear profile that extends across the Sanandaj-Sirjan metamorphic zone in seismic states of Central Iran and Zagros. We compute P receiver functions to investigate crustal and upper mantle discontinuities. We use teleseismic events ( $m_b \geq 5.5$ ,  $30^\circ < \Delta < 95^\circ$ ) registered between 1996 and 2018 and recorded at 10 short-period stations with 3 components and 17 broadband stations with high signal to noise ratio. The observed depth of Moho in the study area is approximately 50 km and rises to 70 km at the end of the seismic linear profile beneath Sanandaj-Sirjan zone. In Central Iran, depths discontinuities in the transition zone are shown by the reference model of deviation, which can be attributed to the convergence of Arabian plate with the Central Iran plateau. Also, the study area was identified as geothermal susceptibility by SUNA and this observation was confirmed.

**Key words:** seismic images, crust, upper mantle, Central Iran, teleseismic waves

## 1. Introduction

The Iranian plateau is part of the Alpine Himalayan orogenic belt. The study area consists of the part of Central Iran and parts of the Zagros Mountain. The Zagros collision zone comprises three major sub-parallel tectonic elements (Fig. 1). They are, from SW to NE, the Zagros Fold and Thrust Belt (Zagros), the Sanandaj-Sirjan Metamorphic Zone (SSZ), and the Urmieh-Dokhtar Magmatic Assemblage (UDMA) (*Stöcklin, 1968; Ricou et al.,*

\*corresponding author: e-mail: f\_farahmand@Qom-iau.ac.ir

1977). The SSZ extending in a narrow long (150–200 km wide) belt is the inner crystalline zone of the Zagros orogen and is parallel to the MZF. The SSZ is bounded to the northeast by the UDMA, which is interpreted as an Andean-type, subduction-related volcanic arc (Berberian and King, 1981). The Central Iranian is constituted of separated blocks that drifted from Gondwana in the Permian to early-Triassic and subsequently accreted onto Eurasia along the Alborz and Kopeh-Dagh sutures during the late Triassic closure of the Paleo-Tethy (Fig. 1) (Falcon, 1974).

The mantle transition zone separates the upper mantle and the lower mantle. The characteristics of the mantle transition zone are crucial for understanding the inner movement of the Earth. The mantle transition zone is bounded by 410 km (Jeffreys, 1936) and 660 km (Niazi and Anderson, 1965) seismic discontinuities. However, the 410 km discontinuity is usually more difficult to detect due to smaller velocity contrast and a regional more com-

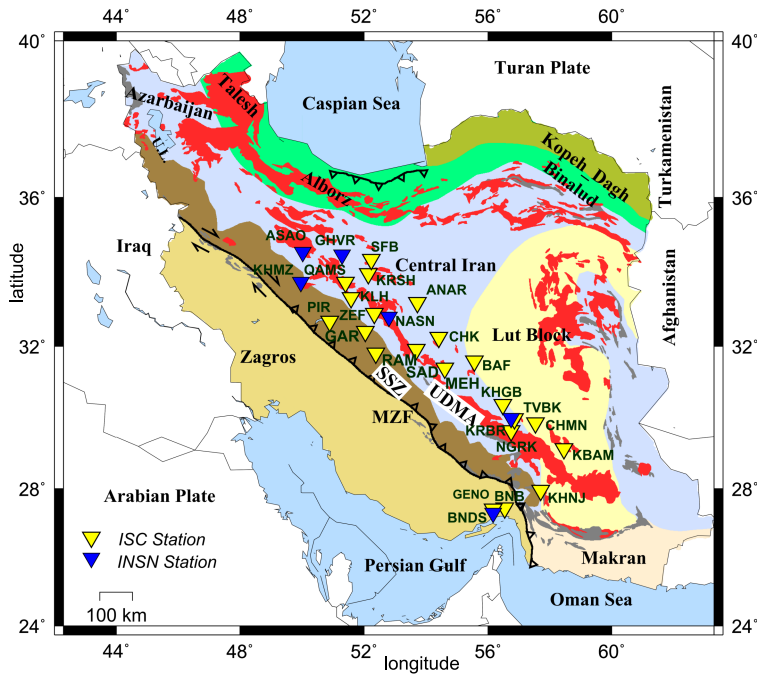


Fig. 1. Main structural units in Iran. Inverse triangles represent 28 seismic stations used in this study. UDMA: Urumieh–Dokhtar Magmatic Arc; SSZ: Sanandaj–Sirjan Zone. Main Zagros Thrust Fault (MZF) is shown in the figure.

plex topography than the 660 km discontinuity (*Bina and Helffrich, 1994; Flanagan and Shearer, 1998b*). Furthermore, locally a weaker discontinuity between them has been observed at a depth 520 km (*Shearer, 1990*). These two main upper mantle discontinuities at 410 km and 660 km indicate the phase transformations in the Olivine component of mantle rock due to increasing pressure. Thermodynamic equilibrium depths depend on the surroundings mantle temperature and pressure conditions, described by the Clapeyron slope (*Suito, 1977*). The Clapeyron slope is defined by the temperature change that causes the phase change with the pressure change. The phase transformations at the 410 km discontinuity have a positive Clapeyron slope and at the 660 km discontinuity have a negative slope. The values of the Clapeyron slope are expressed by *Helffrich (2000)*. If temperature changes occur in the region the phase equilibrium depth will change and the thickness of the mantle transition zone will increase or decrease.

For anomalously cold areas e.g. subducting slabs, 660 km discontinuity is deeper, while 440 km discontinuity is shallower. However, at the same time, the depression of 660 km discontinuity is visible, while the uplift 410 km discontinuity is hard to distinguish (*Gu et al., 1998; Flanagan and Shearer, 1998a,b*). The vertical displacement thickness of the transition zone is calculated through the conversion of the pressure difference to depth (*Stein and Wyession 2003*).

The variation in depth to the 410 km and 660 km discontinuities and the mantle transition zone thickness indicate the local variations in temperature and are a sign of the lateral variation in thermal structure of the mantle transition zone. Therefore studying the depth of these discontinuities will give us a clear understanding of the temperature anomalies that affect the velocity of seismic waves in the upper mantle, deviation from the global model value (*Kennet and Engdahl, 1991*). For more than two decades, the P receiver function method has been used to investigate the structure of the upper mantle discontinuities. Seismic discontinuity is the boundary between two layers with high velocity contrast. This method for studying crust structure in Central Iran has been investigated in several studies with different data (*Paul et al., 2006, 2010; Shad Manaman and Shomali, 2010; Afsari et al., 2011; Mohammadi et al., 2013a; Taghizadeh-Farahmand et al., 2015*). Their results shown the Moho depth in Central Iran changes between 35–55 km and reaches to ~65 km in northern of SSZ. But, there is

little information about the upper mantle transition zone in Central Iran, which is studied by *Rocky and Kaviani (2010)*, *Motaghi et al. (2017)* and *Kaviani et al. (2018)*. All of them indicate that the discontinuities boundary deviates slightly from in the IASP91 velocity model at 410 km and 660 km.

Today, humans have a problem with the supply of clean energy, and geothermal study in Iran (*Yousefi et al., 2007*) has shown that there are areas in our study area that are prone to geothermal energy, so seismic studies can help to confirm study on geothermal-prone areas. Studying the upper mantle and the 410 km and 660 km discontinuity boundaries can be a way to confirm the existence of a heat source inside the earth.

In this study, we use P receiver function method for structure of crust and upper mantle transition zone on a seismic linear profile that continues across Jiroft to Ashtian zone with a suitable distribution of seismic stations parallel to the Main Zagros Fault in the study area compared to previous studies. The location and distribution of seismic stations in this study are shown in Fig. 1.

## 2. Data and method

The study area is located in Central Iran tectonic zone and Zagros zone. In this paper, we used teleseismic P receiver function for estimation of crust thickness depth and upper mantle transition zone thickness under each station. The data used consist of recordings from Tehran (SFB), Esfahan, Yazd, Kerman and Bandar Abbas, three-component telemetry seismic network that were acquired from Iranian Seismographic Center (ISC) of Tehran Geophysics Institute and several broadband telemetry seismic stations of Kerman, Qom, Nain, Khomein and Ashtian were extracted from Iranian National Seismological Network (ISNS) of the International Institute of Earthquake Engineering and Seismology (IIEES). Names and location of these stations are shown in Fig. 1. Teleseismic data were recorded since establishment until 2018. Over 1000 teleseismic events (Fig. 2) whose magnitude exceeded 5.5 mb and epicentral distances ranged from  $30^\circ$  to  $95^\circ$  were utilized in initial stage of PRFs analysis.

Recording mapping with obviously start of P wave and great signal/noise ratio (larger than 4) were chosen at every station from teleseismic earthquake. A good method to locate the discontinuities of the upper mantle

under seismic station is teleseismic receiver function analysis (*Vinnik, 1977; Li et al., 2000a,b*). We applied the P receiver function method to estimate Moho depth and deep mantle discontinuities. A teleseismic P wave that strikes on a discontinuity under a seismic station creates a delayed converted shear wave after the P wave. The temporal difference between conversion of 410 km and 660 km discontinuities relies on the shallow mantle structure. Thus, it reveals transition zone thickness. It is usable to estimate the variation in thickness of the mantle transition zone by comparing this different time with the global average value (24.0 s for the IASP91 model at a reference distance of  $67^\circ$ ). The temperature variation there can happen through change of the thickness of transition zone (*Li et al., 2003*), therefore it is possible to estimate geothermal region in this study.

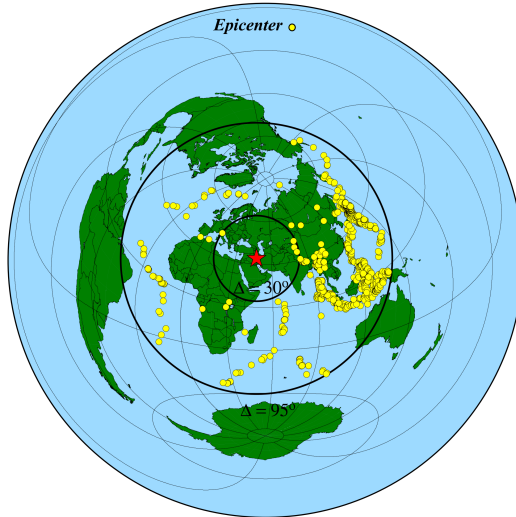


Fig. 2. Distribution of teleseismic events (yellow circles) recorded by seismic network between 1996 and 2018 and used to calculate P receiver functions. The red star shows the approximate position of the network. The black solid circles mark the  $30^\circ$  and  $95^\circ$  epicentral distances, respectively.

A 110 s long time window was considered which begins 10 s prior to 100 s following the P-onset arrival time. The length of the time window is chosen to observe the P to s converted phase in Moho and its multiple reflections. The estimation of PRFs from three-component seismometer includes broadening to response of a short-period instrument into a more

useful teleseismic frequency band, deconvolving the instrument from the original records. The ZNE component wave forms are then rotated into the ZRT coordinate system. The Z component rotated into LQT ray-based coordinate system for isolated P to s conversions from direct P wave. Finally, with deconvolution of the L component from the Q component, P to S conversion is secluded on the Q component. The Q component contains mainly the converted P to s waves and is named P receiver function. A low-pass filter of 2 s is used for the P receiver function. They are stacked after move-out correction for reference slowness of  $6.4 \text{ s}^\circ$ . In addition to the converted phase s the final receiver function contains multiple reflections created by each velocity discontinuity. More information about the exact depth of discontinuity and Poisson's ratio could be obtained by multiple reflections (Yuan *et al.*, 2002; Zhu and Kanamori, 2000; Zandt and Ammon, 1995).

### 3. Observations

The P receiver functions were calculated for all seismic network stations at about 1000 teleseismic earthquakes which were mostly in the back azimuth of  $20^\circ$  to  $130^\circ$ . For each station, we selected the receiver functions that had a visible P-to-S converted phase.

- Kerman seismic network

Kerman broadband seismic network located in the Central Iranian plateau. This network includes 7 stations, from which the 6 stations were useful for calculation of receiver functions. Individual and summation PRFs for station KHGB are presented in Fig. 3. The conversion with the greatest coherence belongs to Moho boundary, emerging with 4.7–7.2 s delay time. The second positive phase (MC) at 3–4 s observed beneath almost all stations can be a discontinuity in the upper crust.

- Isfahan seismic network

Esfahan short period and broadband seismic network is located in the Central Iranian Plateau and Sanandaj-Sirjan zone. Esfahan seismic network includes 9 stations and 8 of them were used to calculate receiver functions. Individual and summation PRFs for station KLH are presented in Fig. 3. Moho converted phase arrived with 5–7 s delay time

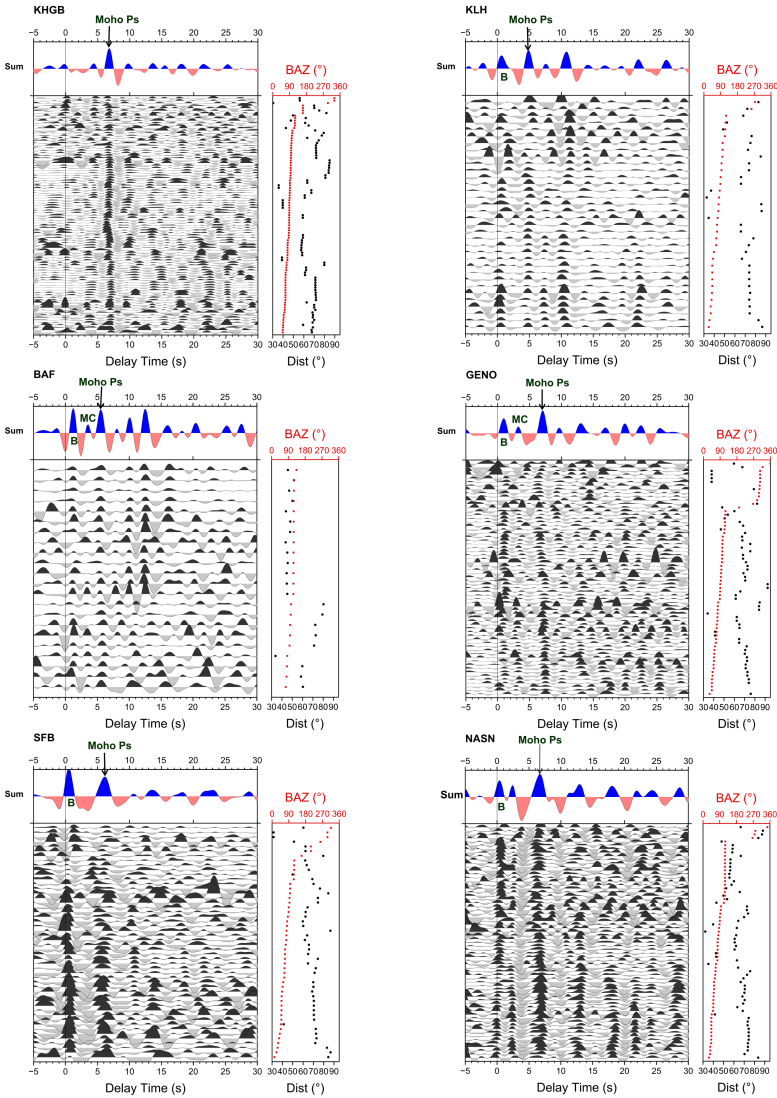


Fig. 3. The receiver functions for seismic network stations were displayed in the time window  $-5$  to  $30$  s which were sorted by increasing back azimuth. Individual PRF with summation traces for some stations in each network are presented. Individual seismograms are plotted equally spaced and sorted by increasing back azimuth (shown in the right). The Ps conversion phases from the sediment ( $1-2$  s, labeled B), the middle crustal layer ( $3-4$ s, labeled MC) and Moho ( $4.7-6.7$ s, labeled Moho Ps) are labelled on the summation traces.

and is observed beneath all stations. The first positive phase (B), which arrives just before the Moho converted phase around 0.5–1 s, is visible at almost all stations. This phase can be a conversion from a sedimentary layer near the surface of the earth. The second positive phase (MC) at about 3–4 s delay time which is observed beneath almost all stations, can be a discontinuity in the upper crust.

- Yazd seismic network

Yazd short period seismic network is located in the Central Iranian plateau. This network includes 5 stations and 2 stations didn't have acceptable data because of high noise. The Moho converted phases can be observed at time ranges between 4.4–6.5 s which is coherent phase at all of the stations. The first positive phase (B) arrives at about 0.5–1 s delay time which can be a sedimentary layer near the surface of the Earth. The second conversion phase (MC) at 3 s delay time which can be seen beneath BAF station (Fig. 3), could be a discontinuity in the crust.

- Minab seismic network

Minab broadband seismic network is located above the strait of Hormoz and southeastern of Zagros zone. Minab seismic network has 3 stations and we calculated receiver function for 2 stations. Individual and summation PRFs for station GENO are presented in Fig. 3. The P–S conversion phases from the Moho at time 5–7 s observed on the summation traces is coherent phase at all of the stations. The first positive phase (B) was observed at about 0.5–1 s delay time, which can be a sedimentary layer near the surface of the earth. The other positive phase (MC) beside the Moho converted phase, which emerged ranging from 2 to 3 s, can be a discontinuity in the crust of the Earth.

- Tehran seismic network

Tehran seismic network is located in the Central Alborz and had 11 stations from which 1 station is within the region of this study. P receiver function at SFB station is shown on Fig. 3. Moho converted phase arrive with 5.6–7.8 s delay time. The first converted positive phase (B) observed at about 0.4–1.6 s can be a surface sedimentary layer.

- Iranian National Seismological Network

We used 6 seismic broadband stations of Iranian National Seismological

Network. The Moho converted phase is observed at time ranges between 4.5–7.2 s delay time. Individual and summation PRFs for station NASN are presented in Fig. 3.

In this study, receiver function forward modelling was used to calculate depth of Moho beneath every station. The results of the P receiver function analysis from recorded teleseismic data in the seismic stations are listed in Table 1, and also the Moho depth variations are shown in Fig. 4.

Table 1. Name of seismic networks, station code, detected time of Ps conversion on Moho (s), observed depth of Moho (km) and number of PRFs for each station.

Network	Station code	Ps Moho time (s)	Moho depth ( $\pm 2$ , km)	No of PRFs
Isfahan	PIR	5.2	44.0	42
	GAR	7.1	60.5	7
	KLH	4.7	40.0	34
	ZEF	6.6	51.0	29
	RAM	6.0	51.0	11
	KRSH	5.0	41.5	57
	QAMS	5.0	41.5	105
Yazd	ANAR	5.6	45.0	30
	BAF	5.5	46.0	22
	CHK	4.4	37.0	23
Kerman	SAD	6.5	54.0	34
	CHMN	7.0	60.0	44
	NGRK	6.3	54.0	33
	KHGB	6.7	57.0	87
	KBAM	7.2	61.0	68
Minab	TVBK	4.8	41.0	24
	GENO	7.0	60.0	58
Tehran	BNB	5.3	43.0	37
	SFB	6.3	50.0	49
INSN	ASAO	6.8	52.0	83
	BNDS	7.2	59.0	58
	GHVR	4.7	37.5	45
	KRBR	5.0	42.0	69
	KHMZ	8.0	65.0	27
	NASN	6.6	54.0	65

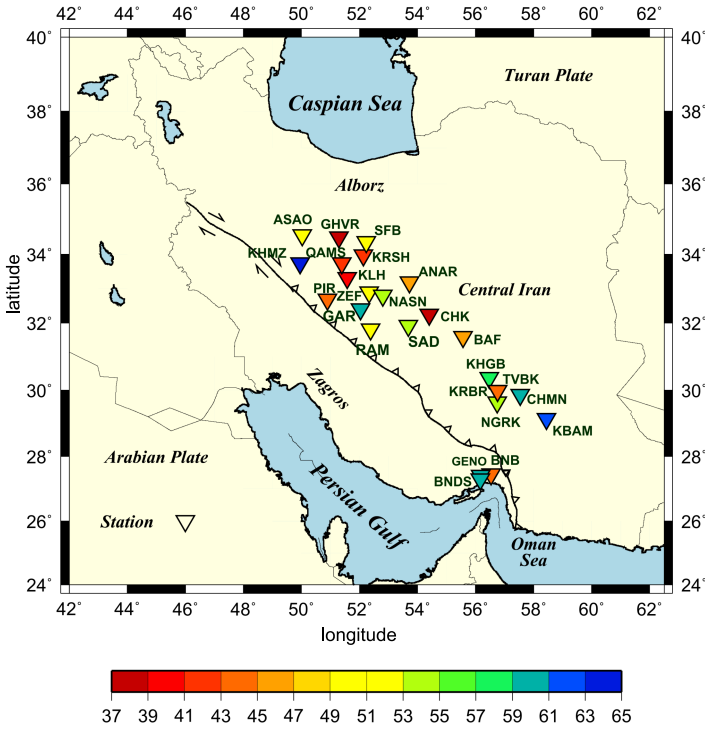


Fig. 4. The map of Moho depth variations in study area.

#### 4. Discussion

We use P receiver functions to map the Moho and the upper mantle 410 km and 660 km discontinuities. For this purpose, we calculated the delay time between converted P to S and direct P than migration of this time delay to depth.

To derive an improved image of the crust beneath the Central Iran, Urumieh-Dokhtar magmatic arc (UDMA) and Sanandaj-Sirjan zone (SSZ), we considered two SW–NE trending profiles (AA' and BB') perpendicular to the strike of the Zagros Mountain belt (Fig. 5).

PRFs were then back projected and migrated into depth along the profiles (refer to Figs. 6 a-b). A 50-km data band from either profile sides was considered for each profile. To migrate from the time domain to the depth domain, we used the IASP91 reference model (Kennett and Engdahl, 1991).

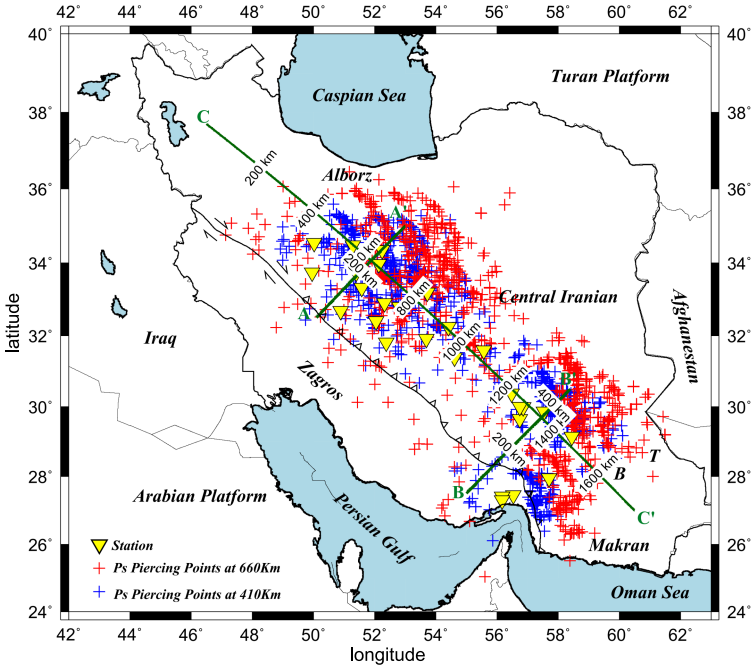


Fig. 5. Location of piercing points (blue and red crosses) of P receiver functions at 410 and 660 km depth, respectively. Green lines mark the location of tow SW–NE and one NW–SE trending profiles used for depth migration. The seismological stations are shown with yellow inverted triangles. The B and T represent the locations of Bazman and Tafttan volcanoes.

The positive amplitudes of receiver functions are plotted red and indicate velocity increase downwards, while blue colour shows negative amplitudes and indicate velocity reduction downwards.

As Figure 6 shows, the Moho depth increases from north-east to south-west. The Moho depth is estimated to be at ~50 km depth along all two profiles with a sudden increase to a depth of about 60–70 km beneath the KHMZ in SSZ (Fig. 6a) These results are in good agreement with those obtained from the detailed P receiver function analysis along profiles crossing the Zagros belt (Paul et al., 2006, 2010; Mohammadi et al., 2013a; Mohammadi et al., 2013b). Also, the Moho depth suddenly increases to a depth of 60–70 km and beneath the GENO and BNDS stations (Fig. 6-b) which is consistent with the results of previous studies (Shad Manaman et al., 2011; Taghizadeh-Farahmand et al., 2015).

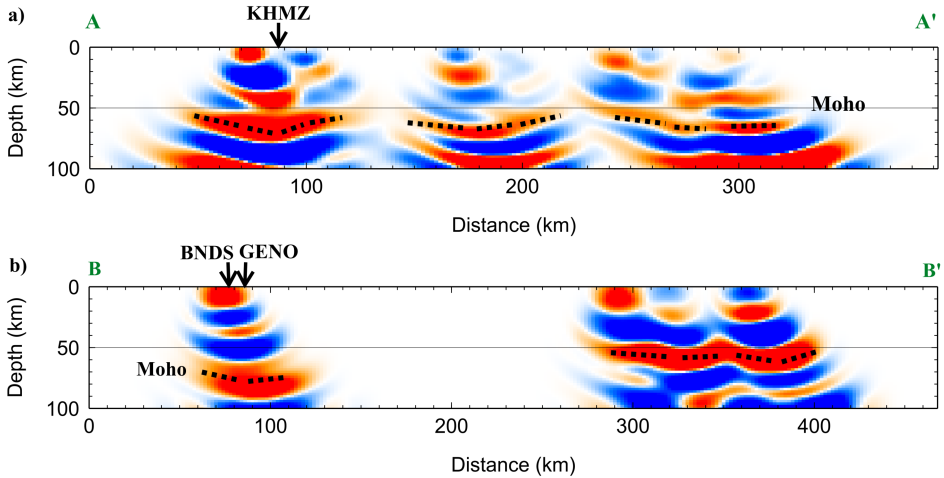


Fig. 6. (a) 2D migrated PRFs along profile AA'. The positive (negative) amplitudes of receiver function are plotted in red (blue). The Moho depth lies at ~55 km with an increasing to about ~70 km towards SW. (b) displays the analogous scheme to (a) along profile BB'. Note the thinnest crust is seen beneath the SW part of profile BB'.

The imaging of transition zone boundaries of 410 km and 660 km are appropriate in the P receiver function depth section, as shown in Fig. 7. This figure displays 2D migrated PRFs together with profile CC' moving through Central Iran, UMDA and SSZ. A 150-km data band from each side of the profile was considered for the profile CC'.

The resultant migrated depth sections of P receiver functions show the crustal thickness about 50 km and an abrupt thickening about 70 km in the starting of profile (C point) in Sanandaj-Sirjan zone that can be well confirmed by the previous PRFs result in this region (e.g., *Sodoudi et al., 2009; Paul et al., 2006, 2010; Afsari et al., 2011; Mohamadi et al., 2013; Taghizade-Farahmand et al., 2015*). Results of *Motaghi et al. (2015, 2017)* studies by receiver function method showed the Moho thickness reaches its maximum in SSZ. According to their velocity model, crustal thickness is increasing beneath the Zagros from 43 km to 50 km (beneath the main fault of Zagros) that gradually has increased beneath SSZ and UDMA and reaches its maximum (62 km) beneath the border of these zones. Also, the crustal thickness is reduced to 42 km beneath Central Iran. These results are according to our study.

The 410 km and 660 km discontinuities are not smooth and include

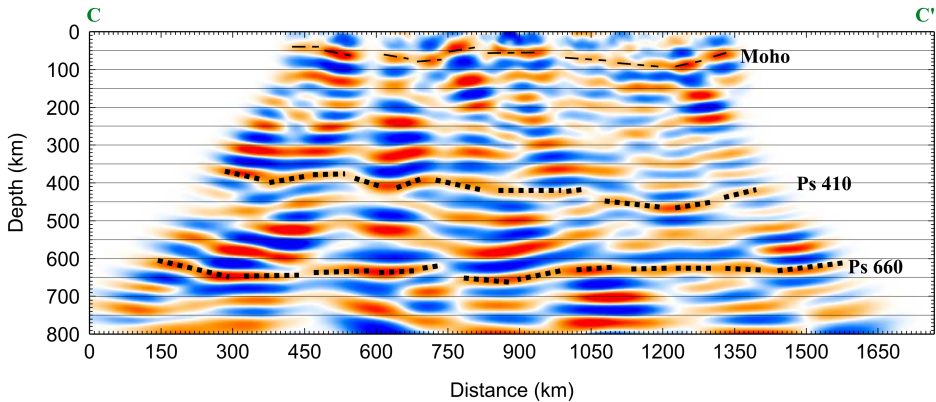


Fig. 7. 2D migrated PRFs along profile  $CC'$ . The positive (negative) amplitudes of receiver function are plotted in red (blue). The Moho depth lies at  $\sim 50$  km with an increasing to about  $\sim 70$  km. The 410 km and 660 km discontinuities are not flat and have anomaly near and under volcanoes that have been derived from the standard IASP91 global earth model.

anomaly in the proximity of volcanoes and beneath them, which have been extracted from the standard IASP91 global earth model. Due to the acceptable depth of Moho in this study, the boundary of discontinuities in the transition zone of the mantle can be considered acceptable. The discontinuities of mantle transition zone are showing deviation from reference model that can be due to velocity variation of P waves beneath this area. The velocity variation may indicate temperature anomalies in the mantle transition zone. Along the  $CC'$  profile, the maximum increase in equilibrium depth at 410 km is about 60 km, about 1200 km from the beginning of the profile, which is equivalent to an increase in temperature of about  $1000^\circ\text{C}$  (as *Helffrich (2000)* model). A decrease in equilibrium depth at 660 km is about 30 km after 600 km and 1200 km from the starting point of the profile, which is equivalent to an increase in temperature of about  $400^\circ\text{C}$ .

According to the studies of *Molinaro et al. (2005)*, *Shad Manaman et al. (2011)* and *Shomali et al. (2011)*, uplift of the asthenospheric material from the shallow mantle due to the fracture of the Arabian subduction plate might be leading to a significant thinning of the lithosphere beneath the northern part of UDMA and Central Iran. This can result in thermal anomalies in the transition zone relative to its adjacent depths. It could also be a reason for the stable Central Iranian plateau. Our studies show a thickening in

the transition zone compared to the reference model (*Kennet and Engdahl, 1991*). This increase in thickness is due to the increase in velocity that can indicate a negative temperature anomaly in the transition zone relative to the ambient which is a consequence of the convergence of the Arabian plate and Central Iran plate. These results confirm previous studies (*Shad Manaman and Shomali, 2010; Rocky and Kaviani, 2010; Shomali et al., 2011*). *Rocky and Kaviani (2010)* and *Kaviani et al. (2018)* interpreted this anomaly (the thickening of the mantle transition zone) as the remnants of the Neo-Tethys ocean, which created a heat shield that prevented heat transfer to the upper layers of the earth and cause abnormal gradient of velocity changes. *Kaviani et al. (2018)* used the method of common conversion point stacking of P wave receiver functions to investigate the topography on the 410 km and 660 km discontinuities. Their results showed that thickness of MTZ is variable in central Iran, a highly depressed 410 km and a normal to slightly uplifted 660 km lead to a thinning of the MTZ. Tomography study by *Alinaghi et al. (2007)* and *Toksöz et al. (2010)* revealed the high-velocity anomaly at the 660 km discontinuity in mantle transition zone and showed an increase in velocity at the 410 km discontinuity beneath Bazman volcano (at the ending of profile CC'). Consequently, a decrease in the equilibrium depth of discontinuities is observed in 2D migrated depth section of PRFs (Fig. 5) beneath the south-east of profile CC'. Along the profile (CC'), the thinning of the transition zone is visible at the end of the profile (C' point), which may be due to the local hot anomaly in upper mantle near Taftan and Bazman volcanoes, this result has also be seen in study by *Kaviani et al. (2018)*.

*Jackson (2000)* in his study explained that low velocity and negative velocity gradient in the upper mantle may illustrate hot and low density upper mantle. *Toksöz et al. (2010)* studies in Iran showed the variation in wave velocity in this region at a depth of 400km and 600km which indicates the temperature anomaly in the depths. Our results from the findings of P receiver function are in line with the findings of previous research.

## 5. Conclusions

P receiver functions analysis findings (gathered from teleseismic incidents at a seismic profile) show clear images from the Moho and upper mantle

discontinuities.

The average depths of Moho are 50 km in observed area which rises toward 70 km beneath the Sanandaj-Sirjan zone (under KHMZ station).

The 410 km and 660 km discontinuities transition zone show deviation from reference model that can be due to temperature anomaly in the mantle transition zone. The maximum deviation of the 410 km discontinuity is about 60 km at 1200 km from the beginning of the seismic profile which is equivalent to an increase in temperature of about 1000 °C. Also, the maximum deviation of the 660 km discontinuity is about 30 km at 600 and 1200 km from the beginning of the seismic profile that is equivalent to a decrease in temperature about 400 °C. Deviations are more visible on the 410 km than on 660 km discontinuity. The thickness of the mantle transition zone beneath Baseman volcano decreases and beneath the other region of this study is increasing which may be due to the convergence of the Arabian plateau with the Central Iranian plateau.

The study of area, which was identified by SUNA/Renewable Energy Organization Iran (<http://www.energyhub.ir>) and *Yousefi et al. (2007)* as a geothermal susceptibility, is also confirmed in the observations of this research.

**Acknowledgements.** Authors are grateful to the Iranian Seismological Center (ISC) and the International Institute of Earthquake Engineering and Seismology (IIEES) for providing the teleseismic waveforms. We used the software packages Seismic Handler (*Stammler, 1993*) for data processing and GMT (*Wessel and Smith, 1998*) for plotting, respectively.

## References

- Afsari N., Sodoudi F., Taghizadeh-Farahmand F., Ghassemi M. R., 2011: Crustal structure of Northwest Zagros (Kermanshah) and Central Iran (Yazd and Isfahan) using teleseismic Ps converted phases. *J. Seismol.*, **15**, 2, 341–353, doi: 10.1007/s10950-011-9227-x.
- Alinaghi A., Koulakov I., Thybo H., 2007: Seismic tomographic imaging of P- and S-waves velocity perturbations in the upper mantle beneath Iran. *Geophys. J. Int.*, **169**, 3, 1089–1102, doi: 10.1111/j.1365-246X.2007.03317.x.
- Berberian M., King G. C. P., 1981: Towards a paleogeography and tectonic evolution of Iran. *Can. J. Earth Sci.*, **18**, 2, 210–265, doi: 10.1139/e81-019.
- Bina C. R., Helffrich G. R., 1994: Phase transition Clapeyron slopes and transition zone seismic discontinuity topography. *J. Geophys. Res. Solid Earth*, **99**, B8, 15853–

- 15860, doi: 10.1029/94JB00462.
- Falcon N. L., 1974: Southern Iran: Zagros mountains. Geol. Soc. Spec. Publ., London, 4, 199–211, doi: 10.1144/GSL.SP.2005.004.01.11.
- Flanagan M. P., Shearer P. M., 1998a: Global mapping of topography on transition zone velocity discontinuities by stacking *SS* precursors. J. Geophys. Res., **103**, B2, 2673–2692, doi: 10.1029/97JB03212.
- Flanagan M. P., Shearer P. M., 1998b: Topography on the 410-km seismic velocity discontinuity near subduction zones from stacking of *sS*, *sP* and *pP* precursors. J. Geophys. Res., **103**, B9, 21165–21182, doi: 10.1029/98JB00595.
- Gu Y., Dziewonski A. M., Agee C. B., 1998: Global de-correlation of the topography of transition zone discontinuities. Earth Planet. Sci. Lett., **157**, 1-2, 57–67, doi: 10.1016/S0012-821X(98)00027-2.
- Helfrich G. R., 2000: Topography of the transition zone seismic discontinuities. Rev. Geophys., **38**, 1, 141–158, doi: 10.1029/1999RG000060.
- Jackson I., 2000: Laboratory measurement of seismic wave dispersion and attenuation: Recent progress. In: Karato S.-I., Forte A., Liebermann R., Masters G., Stixrude L. (Eds.): Earth's Deep Interior: Mineral Physics and Tomography from the Atomic to the Global Scale. American Geophysical Union, Book Series: Geophysical Monograph Series, **117**, 265–289, doi: 10.1029/GM117p0265.
- Jeffreys H., 1936: The structure of the earth down to the 20° discontinuity. Geophys. Suppl. Mon. Not. R. Astron. Soc., **3**, 9, 401–422, doi: 10.1111/j.1365-246X.1936.tb01748.x.
- Kaviani A., Sandvol E., Moradi A., Rümpker G., Tang Z., Mai P. M., 2018: Mantle transition zone thickness beneath the Middle East: Evidence for segmented Tethyan slabs, delaminated lithosphere, and lower mantle upwelling. J. Geophys. Res. Solid Earth, **123**, 6, 4886–4905, doi: 10.1029/2018JB015627.
- Kennett B. L. N., Engdahl E. R., 1991: Travel times for global earthquake location and phase identification. Geophys. J. Int., **105**, 2, 429–465, doi: 10.1111/j.1365-246X.1991.tb06724.x.
- Li X., Kind R., Priestley K., Sobolev S. V., Tilmann F., Yuan X., Weber M., 2000a: Mapping the Hawaiian plume with converted seismic waves. Nature, **405**, 6789, 938–941, doi: 10.1038/35016054.
- Li X., Sobolev S. V., Kind R., Yuan X., Estabrook C., 2000b: A detailed receiver function image of the upper mantle discontinuities in the Japan subduction zone. Earth Planet. Sci. Lett., **183**, 3-4, 527–541, doi: 10.1016/S0012-821X(00)00294-6.
- Li X., Bock G., Vafidis A., Kind R., Harjes H.-P., Hanka W., Wylegalla K., Van der Meijde M., Yuan X., 2003: Receiver function study of Hellenic subduction zone: Imaging crustal thickness variations and the oceanic Moho of the descending African lithosphere. Geophys. J. Int., **155**, 2, 733–748, doi: 10.1046/j.1365-246X.2003.02100.x.
- Mohammadi N., Sodoudi F., Mohammadi E., Sadidkhouy A., 2013a: New constraints on lithospheric thickness of the Iranian Plateau using converted waves. J. Seismol., **17**, 3, 883–895, doi: 10.1007/s10950-013-9359-2.

- Mohammadi E., Sodoudi F., Kind R., Rezapour M., 2013b: Presence of a layered lithosphere beneath the Zagros collision zone. *Tectonophysics*, **608**, 366–375, doi: 10.1016/j.tecto.2013.09.017.
- Molinario M., Zeyen H., Laurencin X., 2005: Lithospheric structure beneath the south-eastern Zagros Mountains, Iran: recent slab break-off? *Terra Nova*, **17**, 1, 1–6, doi: 10.1111/j.1365-3121.2004.00575.x.
- Motaghi K., Tatar M., Priestley K., Romanelli F., Doglioni C., Panza G. F., 2015: The deep structure of the Iranian Plateau. *Gondwana Res.*, **28**, 1, 407–418, doi: 10.1016/j.gr.2014.04.009.
- Motaghi K., Shabanian E., Tatar M., Cuffaro M., Doglioni C., 2017: The south Zagros suture zone in teleseismic images. *Tectonophysics*, **694**, 292–301, doi: 10.1016/j.tecto.2016.11.012.
- Niazi M., Anderson D. L., 1965: Upper mantle structure of western North America from apparent velocities of *P* waves. *J. Geophys. Res.*, **70**, 18, 4633–4640, doi: 10.1029/JZ070i018p04633.
- Paul A., Kaviani A., Hatzfeld D., Vegne J., Mokhtari M., 2006: Seismological evidence for crustal-scale thrusting in the Zagros mountain belt (Iran). *Geophys. J. Int.*, **166**, 1, 227–237, doi: 10.1111/j.1365-246X.2006.02920.x.
- Paul A., Hatzfeld D., Kaviani A., Tatar M., Péquegnat C., 2010: Seismic imaging of the lithospheric structure of the Zagros mountain belt (Iran). *Geol. Soc. Spec. Publ.*, London, **330**, 1, 5–18, doi: 10.1144/SP330.2.
- Rocky M., Kaviani A., 2010: Structure of upper mantle beneath Zagros and Central-Iran obtained from *P* receiver functions: Evidence for subducted oceanic slab break-off. 16th Iranian Geophysical Conference (IGC-16), Tehran University, Tehran, Iran.
- Ricou L. E., Braud J., Brunn J. H., 1977: Le Zagros. *Mém. Soc. Géol. Fr., Hors. Ser.*, **8**, 33–52 (in French).
- Shad Manaman N., Shomali H., 2010: Upper mantle S-velocity structure and Moho depth variations across Zagros belt, Arabian–Eurasian plate boundary. *Phys. Earth Planet. Inter.*, **180**, 1-2, 92–103, doi: 10.1016/j.pepi.2010.01.011.
- Shad Manaman N., Shomali H., Koyi H., 2011: New constraints on upper-mantle S-velocity structure and crustal thickness of the Iranian plateau using partitioned waveform inversion. *Geophys. J. Int.*, **184**, 1, 247–267, doi: 10.1111/j.1365-246X.2010.04822.x.
- Shearer P. M., 1990: Seismic imaging of upper-mantle structure with new evidence for a 520-km discontinuity. *Nature*, **344**, 121–126, doi: 10.1038/344121a0.
- Shomali Z. H., Keshvari F., Hassanzadeh J., Mirzaei N., 2011: Lithospheric structure beneath the Zagros collision zone resolved by non-linear teleseismic tomography. *Geophys. J. Int.*, **187**, 1, 394–406, doi: 10.1111/j.1365-246X.2011.05150.x.
- Sodoudi F., Yuan X., Kind R., Heit B., Sadidkhouy A., 2009: Evidence for a missing crustal root and a thin lithosphere beneath the Central Alborz by receiver function studies. *Geophys. J. Int.*, **177**, 2, 733–742, doi: 10.1111/j.1365-246X.2009.04115.x.

- Stammler K., 1993: Seismichandler—Programmable multichannel data handler for interactive and automatic processing of seismological analyses. *Comput. Geosci.*, **19**, 2, 135–140, doi: 10.1016/0098-3004(93)90110-Q.
- Stein S., Wysession M., 2003: *An Introduction to Seismology, Earthquakes, and Earth Structure*. Blackwell Publishing, 498 p.
- Stöcklin J., 1968: Structural history and tectonics of Iran: A review. *AAPG Bull.*, **52**, 7, 1229–1258, doi: 10.1306/5D25C4A5-16C1-11D7-8645000102C1865D.
- Suito K., 1977: Phase relations of pure Mg<sub>2</sub>SiO<sub>4</sub> up to 200 kilobars. In: Manghnani M., Akimoto S. (Eds.): *High pressure research*. Acad. Press, New York, 255–266.
- Taghizadeh-Farahmand F., Afsari N., Sodoudi F., 2015: Crustal thickness of Iran inferred from converted waves. *Pure Appl. Geophys.*, **172**, 2, 309–331, doi: 10.1007/s00024-014-0901-0.
- Toksöz M. N., van der Hilst R. D., Sun Y., Zhang H., 2010: Seismic tomography of the Arabian-Eurasian collision zone and surrounding areas. Report AFRL-RV-HA-TR-2010-1043, Air Force Research Laboratory, Space Vehicles Directorate, MA USA, 43 p.
- Vinnik L. P., 1977: Detection of waves converted from P to SV in the mantle. *Phys. Earth Planet. Inter.*, **15**, 1, 39–45, doi: 10.1016/0031-9201(77)90008-5.
- Wessel P., Smith W. H. F., 1998: New, improved version of generic mapping tools released. *Eos, Trans. AGU*, **79**, 47, 579, doi: 10.1029/98E000426.
- Yuan X., Sobolev S. V., Kind R., 2002: Moho topography in the central Andes and its geodynamic implications. *Earth Planet. Sci. Lett.*, **199**, 3-4, 389–402, doi: 10.1016/S0012-821X(02)00589-7.
- Yousefi H., Ehara S., Noorollahi Y., 2007: Geothermal potential site selection using GIS in Iran. Proceedings, 32nd Workshop on Geothermal Reservoir Engineering, Stanford University, Stanford, CA, USA, January 22-24, 2007, SGP-TR-183, accessible online from <https://pangea.stanford.edu/ERE/pdf/IGAstandard/SGW/2007/yousefi.pdf>.
- Zandt G., Ammon C. J., 1995: Continental crust composition constrained by measurements of crustal Poisson's ratio. *Nature*, **374**, 152–154, doi: 10.1038/374152a0.
- Zhu L., Kanamori H., 2000: Moho depth variation in southern California from teleseismic receiver functions. *J. Geophys. Res.*, **105**, B2, 2969–2980, doi: 10.1029/1999JB900322.